NASA-CR-191985

Monthly Technical Report.

(NASA-CR-191985) A STUDY OF SOLUTION CRYSTAL GROWTH IN LOW-g Monthly Technical Report, 1 Sep. - 30 Nov. 1992 (Alabama Agricultural and Mechanical Coll.) 23 p

N93-71185

Unclas

Z9/76 0141497

TN-76-CR
141497

2. Recently, the Gen.Rad. Capacitance Bridge 1620A has started giving some erroneous results. It has been sent for repairs and calibration.

3. A computer code is being written to extrapolate various electrical parameters, as mentioned in item No. 1, from our data points at set temperatures of 20 C, 30C, 40C, 45C, 50C, and 60C. This will enable a comparison between all the crystals studied and will alleviate the tedious process of plotting graphs and extrapolating data.

4. Two meetings were held on October 26, 1992 and November 17, 1992 with Mr. Gary Arnett and Miss. Becky Jacobs of CVC, Associates, to discuss the format of g-values plot and time for the IML-1 mission. They have been provided with the hologram numbers and time to determine any unusual g-spikes and values which might have occurred during the mission.

5. All the printouts of sting and fluid temperatures and time have been collected from TBE. They have been plotted and further work is continuing to include the g-values and other significant events during the mission.

6. The TGS solution (pre and post flight) for TGS-1 run for the IML-1 mission and self nucleated TGS crystallites have been chemically analyzed for various metal ion impurities by atomic absorption spectroscopy at SouthEastern Analytical Services, Inc. The results are attached with this report. It is important to note that Nickel contamination in the TGS solution increased from 0.10 mg/l before cell filling to 52.8 mg/l after the IML-1 flight. Thi is a significant contamination in the solution and because of this unintentional nickel doping, the self nucleated crystallites recovered after the flight were found to be needle shaped. This kind of morphology is normally seen in nickel doped TGS crystals. The analysis of the self nucleated crystallites indicates a nickel contamination of about 4.78 mg/l compared to less than 0.10 mg/l in the original solution. This dopant level can be responsible for the needle shaped morphology of the crystallites.

7. On the request of the North American Editor for the special issue on Crystal and Crystal Growth of the journal "Ferroelectrics", an invited review article entitled, " Growth and Properties of Triglycine Sulfate (TGS): Review (65 typed pages) , has been written by R.B. Lal and A.K. Batra and sent for publication.

8. Drs. Lal and Batra attended the Sixth Alabama Materials Research Conference, held at Auburn University, Auburn, Alabama, on October 6-7, 1992 and presented a paper entitled," Growth of Triglycine Sulfate Crystals aboard the First International Microgravity Laboratory (IML-1)". An abstract is enclosed. No proceedings will be published for the conference.

9. Finally, the communication links between HGS, SSL/MSFC, Clarkson University, and MetroLaser have been established. MetroLaser has now the capability to bring an image from MSFC/SSL.

10. Sample disks containing particle image data were sent to Clarkson University to allow them to prepare their image processors and data system to receive the images from NASA/MSFC.

11. A new software has been purchased by MetroLaser in order to characterize the motion of the particles. It will facilitate the calculations of g-values, fluid motion, etc. Details can be seen in attached MetroLaser report.

12. The TGS solution (pre and postflight) and the self nucleated crystallites from the TGS-2 run, which was never accomplished during the IML-1 mission, has been sent for analysis. The crystallites collected from TGS-2 run were found to be prismatic. This will throw more light on the TGS contamination problem.

13. The work at MetroLaser and Clarkson University is progressing well. A report from MetroLaser is enclosed.

14. A paper entitled, " Simulation of Triglycine Sulfate Crystal Growth in Space", by J. Sun, F.M. Carlson, and W.R. Wilcox has been published in Microgravity Q. Vol 2, No. 3, pp 159-168 (1992). A copy is enclosed.

MetroLaser

18006 Skypark Circle, Suite 108, Irvine, CA 92714-6428 Tel: (714) 553-0688 Fax: (714) 553-0495

November 25, 1992

Dr. Ravindra B. Lal
Alabama A & M University
Carter Hall, Physics Department
P.O. Box 71
Normal, Al 35762

RE: NASA Prime Contract NAS8-36634
Our Job No. AL0201

Dear Dr. Lal:

This is the third report for 1992 on the subject contract.

Primary Science Objective

The primary science objective of the particle experiment is to observe and quantify minute convection currents in the vicinity of the crystal and to correlate these with crystal growth processes. With the limited amount of crystal growth data available, we will attempt to observe, isolate, and quantify the following components of fluid convection:

1. Growth driven convection.
2. Convection due to g-jitter.
3. Convection due to other acceleration forces.
4. Convection due to residual microgravity.

All but the first of these was well represented with or without a crystal growing. The three IML-1 runs have been designated as:

Run 1a: Cell #1-Cap did not open.
Run 1b: Cell #1-Cap opened and closed.
Run 2: Cell #2-No data.

Run 1a offers the opportunity to observe particle motion without influence of the crystal.

We will attempt to correlate the presence of convection with other events. Namely, we should be able to more accurately characterize the space shuttle environment, how energy is coupled to an experiment, and its effect on crystal growth.

The primary science objective of the holographic interferometry experiments is to provide a measurement of the concentration and concentration gradients in the vicinity of the crystal to support modeling and to help explain the properties of the resulting crystal.

Secondary Science Objectives:

The dynamics of three ensembles of monodisperse particles in suspension will be observed in microgravity through use of the acquired data. This will provide important basic scientific information about g-jitter, inertial random walk, two phase flow, particle dynamics, and the residual gravitational field in the Spacelab. MetroLaser will be making accurate measurements of convection in a regime never measured before which will allow the validation of both theory and CFD codes.

Summary of work before this period:

MetroLaser has supported Alabama A&M University in the development of the hardware, experiment, experiment planning, simulations, and crew training of this effort. Details of this support have been included in previous reports and will not be included here. During January of 1992, MetroLaser supported the IML-1 mission. The details of the mission support are included in previous reports.

A set of holograms was selected to represent a quiet period during the flight and the rotation of the space shuttle then another level of image reconstruction was made. In this series of tests, approximately 100 transparencies of particle images were made with the help of W. Witherow. With these transparencies a few velocity tracks were made of particles over a time period of approximately four (4) hours. These studies demonstrated that we could measure g and observe a g-jitter type of phenomenon. Values of g in the range from fractions of a micro g to milli g were observed. Various other anomalies were also observed. This effort resulted in photographs, video tapes of particles in motion, particle tracks, and preliminary g- data.

We then worked out a more detailed plan to handle the large quantity of data with the assistance of the Clarkson personnel. Conversations were held with Bill Wilcox and Lya Regal towards this end.

The data volume was divided up into 64 subvolumes of approximately one cubic centimeter each with particle data to be extracted from each volume. A plan was set-up so data could be easily transported to MetroLaser, Clarkson, and Alabama A&M University.

Work performed during this period:

Data Reduction/ Interpretation Plan

A detailed plan was worked out to extract data from all of the holograms and was described in the last report. Since that time, the number of digitized images has increased. The table below shows the new number.

Run no.	No. of holograms	Images/hologram	No. of Images
1a	43	18	768
1b	62	64	3968
1b	62	1 interferogram	62
		Total	4798

The images of particle fields and interferograms will be digitized in the HGS and will be transferred over the NASA ethernet or internet system to the SSL VAX and stored on the SSL Write once, read many (WORM) drive. The VAX will be addressable by designated groups who will be able to access the digitized images through the use of internet. It is assumed that MetroLaser and Clarkson will be able to access the SSL VAX and transport the images into their own image processors. In order to have access, a group must have access to internet and have File Transfer Protocol (FTP) capability.

A meeting was held on 15 October to review the status of the data reduction. During the meeting it was found that while most of the images had been digitized, it had been done in such a manner that registration between frames would not be possible. Therefore, the data, (except for that which had constant reference markers in it), would not be usable for most of the particle motion analysis since particles could not be tracked between frames. Dave McIntosh agreed to repeat the data digitization.

A set of action items was developed to put the data reduction process in operation. This requires establishing communication links between HGS, SSL,

Clarkson, and MetroLaser. These links have now been established. MetroLaser now has the capability to bring in an image from SSL.

Data digitizing was repeated only to discover that a problem in the traverse still prevented accurate registration of the frames from separate holograms. A new plan was developed between Dave McIntosh and MetroLaser that would correct this problem. This requires scanning only a single plane in each hologram before switching to the next hologram. Although this will require considerable additional labor at HGS, we could not come up with an alternative solution. Dave McIntosh agreed to repeat the data digitization for a third time.

As soon as W. Witherow receives the data, he is prepared to copy it into the WORM drive.

Sample disks containing particle images were sent to Clarkson to allow them to prepare their image processors and data system to receive the images from NASA. MetroLaser communicated with Fred Carlson at Clarkson on several occasions to assist them in their preparation.

MetroLaser has evaluated a variety of image processing schemes for tracking particles. Meetings were held with the UCI Computer Sciences department and with Imaging Technology Inc. to discuss the problem. Werner Frei Associates is a local company which specializes in the development of software for the imaging technology frame grabber. After holding meetings with this group, we concluded that an existing software package called "ImageLab" could be purchased for approximately $7,000 and modified by W.F. Associates to perform precisely the task which is needed for particle tracking. Towards this end, MetroLaser has written a set of specifications for the software modification and negotiated with W.F. Associates to make the modification. We have now acquired the modified software and installed it in an in-house computer. We have performed the preliminary check-out of the system on particle data collected in earlier recordings where registration required an in-picture reference point (e.g. the crystal).

The program works in the following way:

An image is called onto the screen where a variety of image processing can be performed to clean up the image. For example, all images outside a selected size range can be removed. Any other marked noise can be rejected. Edge enhancement, contrast changes, thresholding, etc., can also be done, if needed. A number of particles to track is selected. One by one, the particle centers are marked then the program numbers and marks the particle center. The next image in the sequence is called up. By toggling back and forth between the first and second image, the corresponding numbered particles are marked in the second

image. The particle xy positions and particle number are stored in the computer memory and the next image is called up. The same process goes on for as long as the selected set of particles can be tracked.

After several hours of data are recorded, the image data is transferred to a speadsheet and plotting program which plots out the particle track and computes the various parameters, such as velocity, g, g-jitter, etc.

A preliminary data set has been produced which appears similar to data produced earlier using photographs. This tests appears to demonstrate that we can produce high quality data without going through the expensive and cumbersome photographic process.

Work Planned for Next Period:

The next period will be spent in extracting particle images and working with Clarkson University to interpret the data.

Please contact me should you have any questions.

Sincerely,

James D. Trolinger, Ph.D.
Director of Research
MetroLaser

SouthEastern
SEAS
ANALYTICAL SERVICES, INC.
1004 OSTER DR., SUITE 1 • HUNTSVILLE, ALABAMA 35816 • 205 / 536-8110

Wed Nov 4 1992

Laboratory Report

Client: Alabama A&M University
P.O. Box 71
Normal, AL 35762

Attn: Dr. Batra

Sample ID: #3 Crystallites out of FES#1
Date Received: 10/27/1992
Purchase Order No.: 36909

Lab. No.: 0161-3012-03

Parameter	Results	Method	Analyst	Date	Time
Copper(T)	< 0.22 ug/g	305	db	11-03-92	1200
Lead (T)	< 1.09 ug/g	305	db	11-03-92	1200
Chromium (T)	< 0.55 ug/g	305	db	11-03-92	1200
Barium (T)	< 0.22 ug/g	305	db	11-03-92	1200
Nickel (T)	4.78 ug/g	305	db	11-03-92	1200
Sodium (T)	9.73 ug/g	305	db	11-03-92	1200
Manganese (T)	< 0.22 ug/g	305	db	11-03-92	1200
Zinc (T)	2.70 ug/g	305	db	11-03-92	1200
Iron (T)	0.97 ug/g	305	db	11-03-92	1200
Silicon (T)	4.37 ug/g	305	db	11-03-92	1200
Magnesium (T)	1.29 ug/g	305	db	11-03-92	1200
Aluminum (T)	1.50 ug/g	305	db	11-03-92	1200
Gold (T)	< 0.11 ug/g	305	db	11-03-92	1200
Thallium (T)	< 1.09 ug/g	305	db	11-03-92	1200

Method Sources
EPA-Test Methods for Evaluating Solid Waste, SW-846 3rd Ed.
EPA-Methods for Chemical Analysis of Water and Wastes (1983)
Standard Methods for the Examination of Water and Wastewater, 16th Ed.
40 CFR Part 136

Respectfully submitted,

Guy E. Graves, Ph.D.
Vice President

SouthEastern
SEAS
ANALYTICAL SERVICES, INC.
1004 OSTER DR., SUITE 1 • HUNTSVILLE, ALABAMA 35816 • 205 / 536-8110

Wed Nov 4 1992

Laboratory Report

Client: Alabama A&M University
P.O. Box 71
Normal, AL 35762

Attn: Dr. Batra

Sample ID: 1-92 Solution used to fill the Cell
Date Received: 10/27/1992
Purchase Order No.: 36909

Lab. No.: 0161-3012-01

Parameter	Results	Method	Analyst	Date	Time
Copper(T)	0.32 mg/L	305	db	11-03-92	1200
Lead (T)	< 0.10 mg/L	305	db	11-03-92	1200
Chromium (T)	< 0.05 mg/L	305	db	11-03-92	1200
Barium (T)	0.11 mg/L	305	db	11-03-92	1200
Nickel (T)	< 0.10 mg/l	305	db	11-03-92	1200
Sodium (T)	4.78 mg/L	305	db	11-03-92	1200
Manganese (T)	< 0.02 mg/L	305	db	11-03-92	1200
Zinc (T)	38.6 mg/L	305	db	11-03-92	1200
Iron (T)	0.71 mg/L	305	db	11-03-92	1200
Silicon (T)	2.06 mg/L	305	db	11-03-92	1200
Magnesium (T)	2.96 mg/L	305	db	11-03-92	1200
Aluminum (T)	2.76 mg/L	305	db	11-03-92	1200
Gold (T)	< 0.01 mg/L	305	db	11-03-92	1200
Thallium (T)	< 0.10 mg/L	305	db	11-03-92	1200

Method Sources
EPA-Test Methods for Evaluating Solid Waste, SW-846 3rd Ed.
EPA-Methods for Chemical Analysis of Water and Wastes (1983)
Standard Methods for the Examination of Water and Wastewater, 16th Ed.
40 CFR Part 136

Respectfully submitted,

Guy E. Graves, Ph.D.
Vice President

SouthEastern
SEAS
ANALYTICAL SERVICES, INC.
1004 OSTER DR., SUITE 1 • HUNTSVILLE, ALABAMA 35816 • 205 / 536-8110

Wed Nov 4 1992

Laboratory Report

Client: Alabama A&M University
P.O. Box 71
Normal, AL 35762

Attn: Dr. Batra

Sample ID: 2-92 Solution after the flight
Date Received: 10/27/1992
Purchase Order No.: 36909

Lab. No.: 0161-3012-02

Parameter	Results	Method	Analyst	Date	Time
Copper (T)	0.03 mg/L	305	db	11-03-92	1200
Lead (T)	< 0.10 mg/L	305	db	11-03-92	1200
Chromium (T)	1.99 mg/L	305	db	11-03-92	1200
Barium (T)	0.03 mg/L	305	db	11-03-92	1200
Nickel (T)	52.8 mg/L	305	db	11-03-92	1200
Sodium (T)	4.01 mg/L	305	db	11-03-92	1200
Manganese (T)	0.34 mg/L	305	db	11-03-92	1200
Zinc (T)	52.1 mg/L	305	db	11-03-92	1200
Iron (T)	9.34 mg/L	305	db	11-03-92	1200
Silicon (T)	9.07 mg/L	305	db	11-03-92	1200
Magnesium (T)	3.97 mg/L	305	db	11-03-92	1200
Aluminum (T)	4.18 mg/L	305	db	11-03-92	1200
Gold (T)	< 0.01 mg/L	305	db	11-03-92	1200
Thallium (T)	< 0.10 mg/L	305	db	11-03-92	1200

Method Sources
EPA-Test Methods for Evaluating Solid Waste, SW-846 3rd Ed.
EPA-Methods for Chemical Analysis of Water and Wastes (1983)
Standard Methods for the Examination of Water and Waste-water, 16th Ed.
40 CFR Part 136

Respectfully submitted,

Guy E. Graves, Ph.D.
Vice President

SouthEastern
SEAS
ANALYTICAL SERVICES, INC.
1004 OSTER DR., SUITE 1 • HUNTSVILLE, ALABAMA 35816 • 205 / 536-8110

Wed Nov 4 1992

Laboratory Report

Client: Alabama A&M University
P.O. Box 71
Normal, AL 35762

Attn: Dr. Batra

Sample ID: #3 Crystallites out of FES#1
Date Received: 10/27/1992
Purchase Order No.: 36909

Lab. No.: 0161-3012-03

Parameter	Results	Method	Analyst	Date	Time
Copper(T)	< 0.22 ug/g	305	db	11-03-92	1200
Lead (T)	< 1.09 ug/g	305	db	11-03-92	1200
Chromium (T)	< 0.55 ug/g	305	db	11-03-92	1200
Barium (T)	< 0.22 ug/g	305	db	11-03-92	1200
Nickel (T)	4.78 ug/g	305	db	11-03-92	1200
Sodium (T)	9.73 ug/g	305	db	11-03-92	1200
Manganese (T)	< 0.22 ug/g	305	db	11-03-92	1200
Zinc (T)	2.70 ug/g	305	db	11-03-92	1200
Iron (T)	0.97 ug/g	305	db	11-03-92	1200
Silicon (T)	4.37 ug/g	305	db	11-03-92	1200
Magnesium (T)	1.29 ug/g	305	db	11-03-92	1200
Aluminum (T)	1.50 ug/g	305	db	11-03-92	1200
Gold (T)	< 0.11 ug/g	305	db	11-03-92	1200
Thallium (T)	< 1.09 ug/g	305	db	11-03-92	1200

Method Sources
EPA-Test Methods for Evaluating Solid Waste, SW-846 3rd Ed.
EPA-Methods for Chemical Analysis of Water and Wastes (1983)
Standard Methods for the Examination of Water and Waste-water, 16th Ed.
40 CFR Part 136

Respectfully submitted,

Guy E. Graves, Ph.D.
Vice President

SouthEastern
SEAS
ANALYTICAL SERVICES, INC.
1004 OSTER DR., SUITE 1 • HUNTSVILLE, ALABAMA 35816 • 205 / 536-8110

Fri Dec 4 1992

Laboratory Report

Client: Alabama A&M University
P.O. Box 1268
Normal, AL 35762

Attn: A.K. Batra

Date Received: 12/01/1992
Workorder No.:0161-3362
Purchase Order No.:

Parameter	Results	Method	Analyst	Date	Time
1-92					
Titanium (T)	< 0.10 mg/L	6010	db	12-03-92	1630
2-92					
Titanium (T)	1.15 mg/L	6010	db	12-03-92	1630
3-92					
Titanium (T)	< 1.49 ug/g	6010	db	12-03-92	1630

Respectfully submitted,

Guy E. Graves, Ph.D.
Vice President

Growth of Triglycine Sulfate Crystals aboard First International Microgravity Laboratory (IML-1)*

R. B. Lal and A. K. Batra
Department of Physics
Alabama A&M University
P. O. Box 71, Huntsville, AL 35762
Tel. No. : 205-851-5306
FAX : 205-851-7984

W. R. Wilcox,
Clarkson University,
J. D. Trolinger
MetroLaser,
B. Steiner
NIST,
and
W. R. Witherow
NASA, Marshall Space Flight Center

Abstract

An experiment entitled, "A study of solution crystal growth in low-g," was flown on STS-42 on the First International Microgravity Laboratory (IML-1) on January 22-29, 1992. The objects of the experiment are: a) to grow crystals of triglycine sulfate (TGS) by solution crystal growth technique using modified Fluid Experiment System (FES); b) to perform holographic tomography of the fluid in three dimensions; c) to study the fluid motion due to g-jitter by multiple exposure holography of tracer particles; and d) to study the influence of g-jitter on the growth rate. A TGS crystal was grown on a (010) oriented seed crystal with flat face dimension of about 1 cm and thickness of 3.5 mm. Polystyrene particles of three different sizes, 199μm, 468μm, and 646μm were used to study the fluid motion using holographic technique. The growth on (010) face was found to be substantially uniform. An initial examination of the space crystal by x-ray diffraction synchrotron radiation imaging technique indicates that the lattice orientation is uniform to 1-2 arc seconds locally, and limited by the seed uniformity to 8 arc seconds for the entire crystal. No prominent growth related screw dislocations are seen. The interface between the seed and new growth is scarcely visible. Fluid motion is detected by tracking of particles from one hologram to the next. Preliminary data for the infrared detectivity (D*) for I. R. detectors fabricated from space crystal indicates improved detectivity compared to ground based crystals.

* Work supported by National Aeronautics and Space Administration Office of Microgravity Science and Applications Division, NASA Headquarters.

Presented at 6th Alabama Materials Research Conference, Auburn University, Auburn, AL, October 6-7, 1992.

Microgravity Q. Vol. 2, No. 3, pp. 159–168, 1992
Printed in Great Britain. All rights reserved

0958-5036/92 $5.00 + 0.00
Copyright © 1992 Pergamon Press Ltd

SIMULATION OF TRIGLYCINE SULFATE CRYSTAL GROWTH IN SPACE

JIANHUA SUN, FREDERICK M. CARLSON and WILLIAM R. WILCOX
Department of Mechanical and Aeronautical Engineering, and Center for Crystal Growth in Space, Clarkson University, Potsdam, NY 13699, U.S.A.

Abstract—The Space shuttle environment is not completely gravity-free. Both the steady and fluctuating (jitter) components of the g field are important factors to be considered when lengthy space experiments are performed. By computer simulation of solution crystal growth under such conditions, it was found that the initial thermal convection quickly changes into a solutally-dominated buoyancy-driven flow that is strong enough to influence the concentration distribution. The time needed for buoyancy-driven convection to become important enough to influence the growth rate depends on the magnitude of g. Under steady g, the predicted crystal morphology is related to the orientation of g. The average growth rate is mainly affected by the magnitude of g. Sinusoidal g-jitter at a frequency lower than 0.01 Hz increases the mass transport and therefore the growth rate. The temperature at the seed crystal dominates and determines the growth rate; thus isothermal cooling is not necessary. Use of a fast growing face increases the growth rate by only 10–20% compared to use of a slow growing face, indicating that growth is primarily transport controlled.

1. INTRODUCTION

Triglycine sulfate (TGS) crystals have great technological importance as infrared detection materials. It is also a good model material for crystal growth from solution in space [1]. The first flight experiment was done in Spacelab-3 in 1985. Another flight experiment was recently performed in the first International Microgravity Laboratory (IML-1) on Space Shuttle Discovery [2].

One objective of crystal growth in space is to remove gravity-related effects that limit the perfection of crystals. However, experiments in the Space Shuttle are subjected to some gravity-like accelerations referred to as "microgravity" [3–5]. Thus, the growth process may still include some buoyancy-driven convection instead of being purely diffusive. This can be seen from the experimental results in Spacelab-3, where the solute concentration eventually deviated from a symmetric distribution [6]. Other analytical and numerical work also has examined the significance of convection in crystal growth in space [7]. Since buoyancy-driven convection influences growth kinetics, compositional homogeneity, impurity distribution, morphological stability and nucleation [8], the convection due to microgravity becomes an important factor to consider when space experiments are planned.

The first objective of the present work was to determine the effects of microgravity on TGS crystal growth in space by computer simulation. The second objective was to design control parameters for a flight experiment.

Several models and simulations have already been performed for TGS crystal growth in space, including models for the concentration field and the growing crystal interface. Liu *et al.* [9] modelled pure diffusion using one-dimensional spherical coordinates before the flight experiment in Spacelab-3. Yoo *et al.* [10] later considered pure diffusion using cylindrical coordinates. Yoo's mathematical model and numerical simulation could not explain the non-symmetric concentration field or the larger growth rate than predicted in the space experiment. They speculated that the time for convection to influence the growth grate depends on the magnitude of g and that g-jitter can accelerate the growth rate.

Nadarajah *et al.* [11] used dimensionless Navier–Stokes equations in the 2-dimensional Boussinesq form. They found that the weak convection due to microgravity can result in large non-uniformities in the concentration field near the crystal, with corresponding spatial variations in the growth rate.

In the present work the general form of the Navier–Stokes equations [9] was applied to the bulk solution. The growth equation at the interface was based on the concentration gradient normal to the crystal surface. With the help of a modified finite control volume code, many two dimensional cases under microgravity conditions were simulated. The results showed that microgravity does influence the TGS growth process through solutally dominated buoyancy-driven convection. The orientation and magnitude of the background g play different roles in the crystal morphology and the growth rate. g-Jitter at low frequencies can cause fluctuating growth. g-Jitter also increases the transport and therefore the growth rate. By these simulations we found some effective ways to improve the growth process in order to obtain the best quality crystal.

PRECEDING PAGE BLANK NOT FILMED

PRECEDING PAGE BLANK NOT FILMED

2.3. Other boundary conditions

The conditions at boundaries other than the interface are non-slip, adiabatic, temperature specified and impermeable, i.e.

$$V_f = 0, \tag{10}$$

$$\frac{\partial T_f}{\partial n} = 0 \quad \text{or} \quad T_f = T_w(t) \tag{11}$$

$$\frac{\partial C_f}{\partial n} = 0. \tag{12}$$

3. NUMERICAL SIMULATION

A finite control volume code, "COMMIX-1B" developed at Argonne National Laboratory [13], was modified to include the mass transfer and the growth interface model. A TGS material property library was also established to use in the program.

3.1. Microgravity environment

The microgravity environment is comprised of various disturbances, such as gravitional field variation along the orbit, residual force at locations other than the center of mass, drag, operational activities, motion of mechanical parts or crew activities, etc. For convenience, this environment is usually characterized as a steady background g and a fluctuating g-jitter. By Fourier transformation, the g signals can be decomposed into a series of sinusoidal signals with different magnitudes and frequencies, i.e.

$$g_j = g_{j0} + \sum_{m=1}^{\infty} g_{jm} \sin(2\pi f_{jm} + \varphi_{jm}) \quad (j = 1, 2, 3). \tag{13}$$

The g vector is three dimensional. In our simulations, however, only those orientations perpendicular or parallel to the exposed crystal interface were applied. The effects of the steady component and sinusoidal components were considered separately. For the background g, the magnitude was chosen to be between 10^{-7} and $10^{-4}\,g_0$ (g_0 is Earth's gravity). Usually, space vehicles in orbit are either in the inertial mode or in the gravity-gradient mode. Therefore, the orientation of the background g relative to the experimental devices could be rotating or fixed, respectively. For g-jitter, the magnitude is typically on the order of $10^{-3}\,g_0$ at frequencies from 10^{-3} to 50 Hz. Since the computational cost for simulating real g-jitter is painful when very small time steps are needed, this work was limited to a single sinusoidal mode. It is felt that this simplification retains the essence of the transport mechanisms.

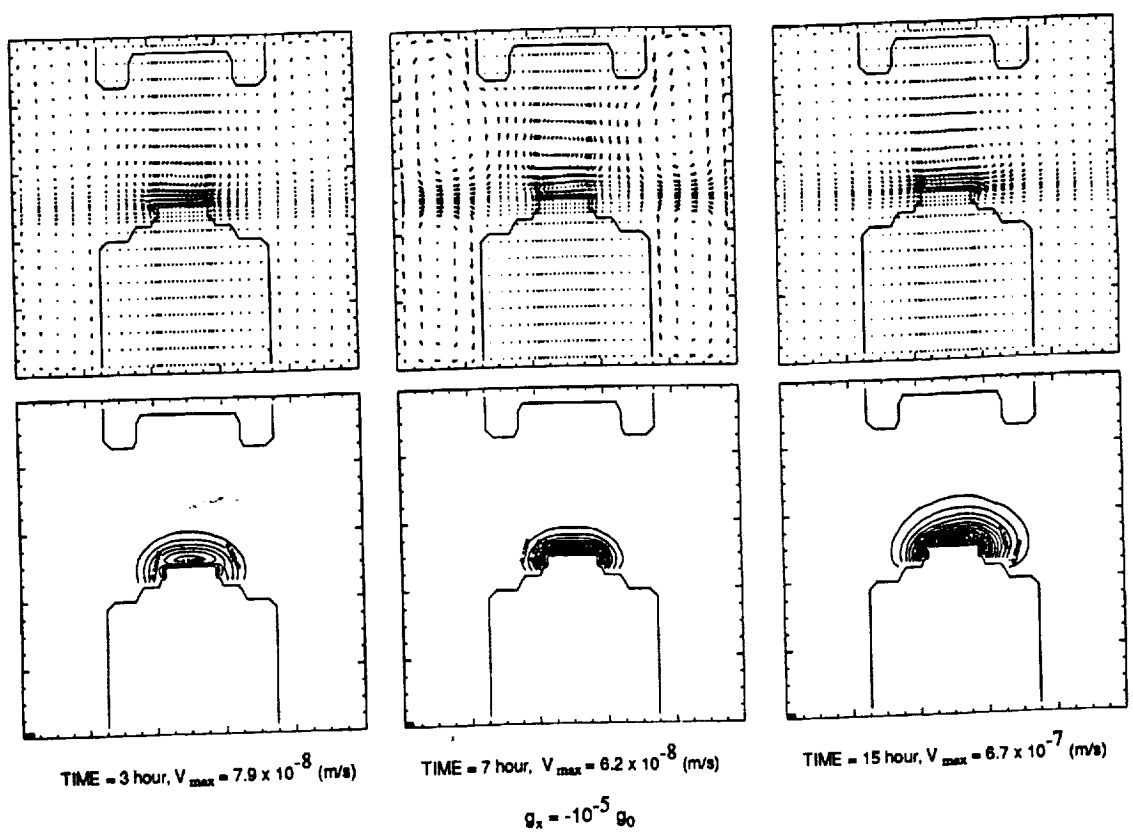

Fig. 2. Transition from thermal convection to solutally dominated convection—velocity and concentration. The (001) face is exposed. The sting and the wall are cooled at a constant rate of 0.42°C/h for 50 h.

4.1. Other considerations

The material properties and TGS solubility were expressed numerically as functions of T and C according to the experimental work of Kroes *et al.* [16, 17]. The kinetic coefficient K_c is 1.0 mm/day · °C for the (001) face and 2.0 mm/day · °C for the (010) face.

As indicated by Nadarajah *et al.*, using the diffusivity obtained by Kroes *et al.* might lead to an overestimation of the growth rate, because their diffusivity was determined only as a function of temperature using a dilute solution. In our case, the solution was in the supersaturated state. It is known that diffusivities typically decline dramatically with increasing concentration in supersaturated solutions [18].

A 38 × 28 grid was used with denser spacing near the interface. The time steps were chosen as 600 s for steady background g and 1/20 of the period of the sinusoidal fluctuating component for g-jitter.

4. RESULTS AND DISCUSSION

The process planned for TGS growth in space was as follows. At the start of an experiment, the initial temperature of the solution was to be 46°C (1°C above the saturation temperature of 45°C). The crystal began to dissolve, causing the concentration and the density of the solution in the vicinity of the seed crystal to increase. At the same time, because the temperatures on the sting and wall were lowered at a controlled cooling rate (say, 0.42°C/h), very weak thermal convection appeared in the growth cell. The dissolution continued for 1–2 h and then transited to crystallization. The previously dissolved solute around the crystal then was gradually reabsorbed. The fluid flow also changed from thermal convection to solutally dominated convection. This process required 5–8 h. As the sting and the wall were further cooled, the convection became stronger and began to deform the sphere-like concentration field. Thus, the concentration gradient and therefore the growth rate along the interface were influenced by the convection. The time for the transition from dissolution to crystallization was mainly controlled by the cooling rate of the sting. The time for transition from thermal convection to solutal convection depended on both the cooling rate of the sting and the microgravity conditions.

4.1. Gravity-gradient mode

For a Space Shuttle in the gravity-gradient mode, where the background g is in a fixed direction, Fig. 2 shows typical velocity and concentration fields during the transition from thermal convection to solutal convection. Although different flow patterns and concentration distributions are determined by the steady background g (i.e. both the orientation and the magnitude), these transition processes are basically similar to each other.

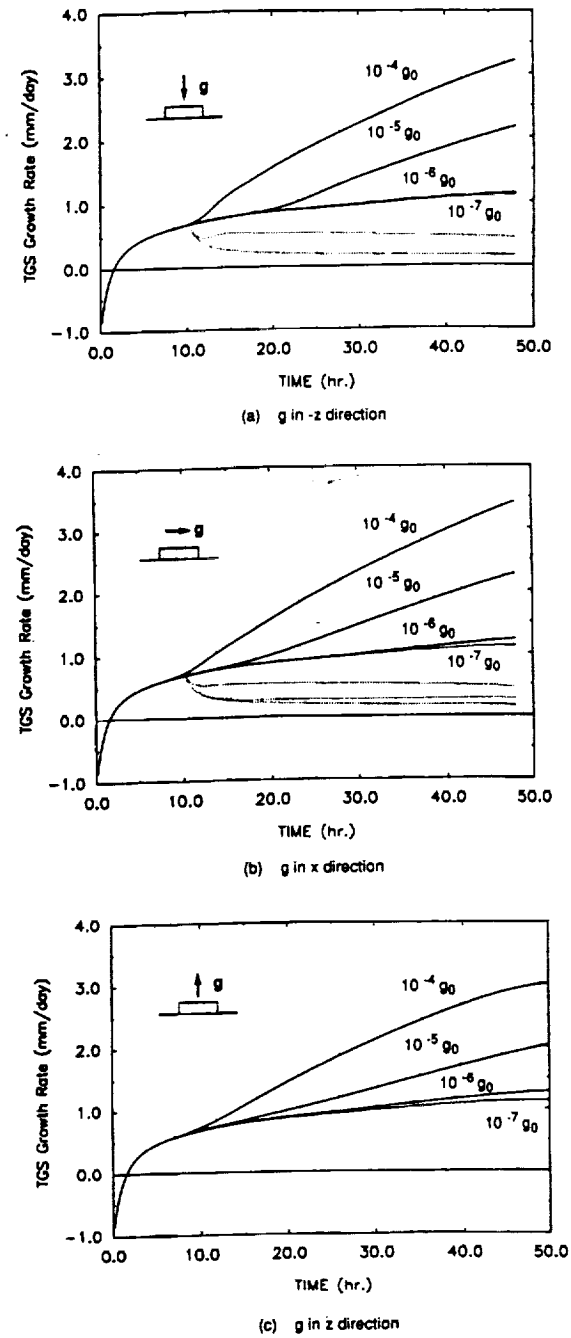

Fig. 3 Average TGS growth rate of the face (001) with different orientations and magnitudes of the steady background g. (——) The sting and the wall both cooled at a constant rate of 0.42°C/h for 50 h. (-----) The sting and the wall both cooled at the constant rate of 0.42°C/h for 10 h and then held at that temperature.

After 10 h of growth, the convection is still quite small, even if the steady g is as high as $10^{-4} g_0$. This can be seen in Fig. 3, which shows the average growth rate of the face (001) under different g levels with a constant cooling rate of 0.42°C/h for 50 h. The convection takes time to become strong enough to influence the growth rate. Its observable effects

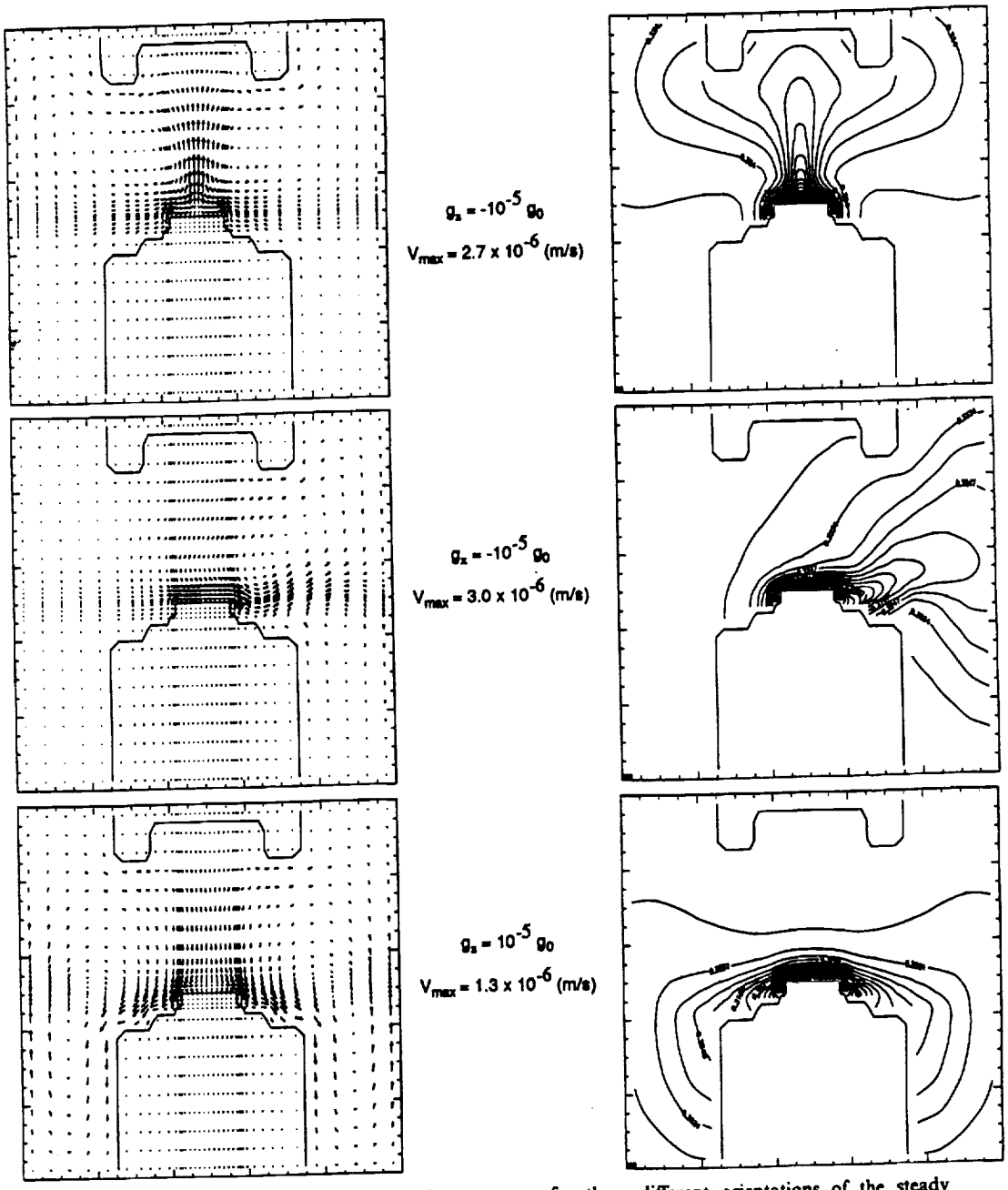

Fig. 4. Velocity profiles and concentration contours for three different orientations of the steady background g at 45 h since the experiment is started. The sting and wall are cooled at a constant rate of 0.42°C/h for 50 h. The (001) face is exposed.

depend on the g level. The larger is g, the more the growth rate is increased; the larger is g, the less time before convection influences the growth rate. For g less than $10^{-6}\ g_0$, the convection is predicted to be too small to influence the growth rate during the first 50 h. This inicates that for long space experiments, the effects of buoyancy-driven convection must be considered.

Comparing (a) to (b) and (c) in Fig. 3, it is seen that the average growth rate depends only slightly on the orientation of the steady background g. However, the orientation plays an important role in generating the flow patterns, concentration distributions, and the variation in growth rate along the crystal surface. Figure 4 presents the velocity profile and the concentration contour at 45 h with the background g in three different orientations. Figure 5 presents the corresponding growth rate along the growth interface versus time. When the steady background g is normal to and pointing toward the exposed face of the seed, solutally dominated convection leads to a higher concentration gradient at the corners than at the center of the face. The growth rate has a similar distribution, causing the grown crystal to have a

concave surface and sharp corners. When the steady g is oriented parallel to the exposed interface, the corner effects mentioned above are much reduced, because the convection sweeps parallel to the interface. Since the nutrient solution is depleted during its passage over the crystal face, the grown crystal becomes non-symmetric. When the steady g vector points in the normal direction away from the exposed interface, the nutrient solution flows towards the center of the face. The growth rate

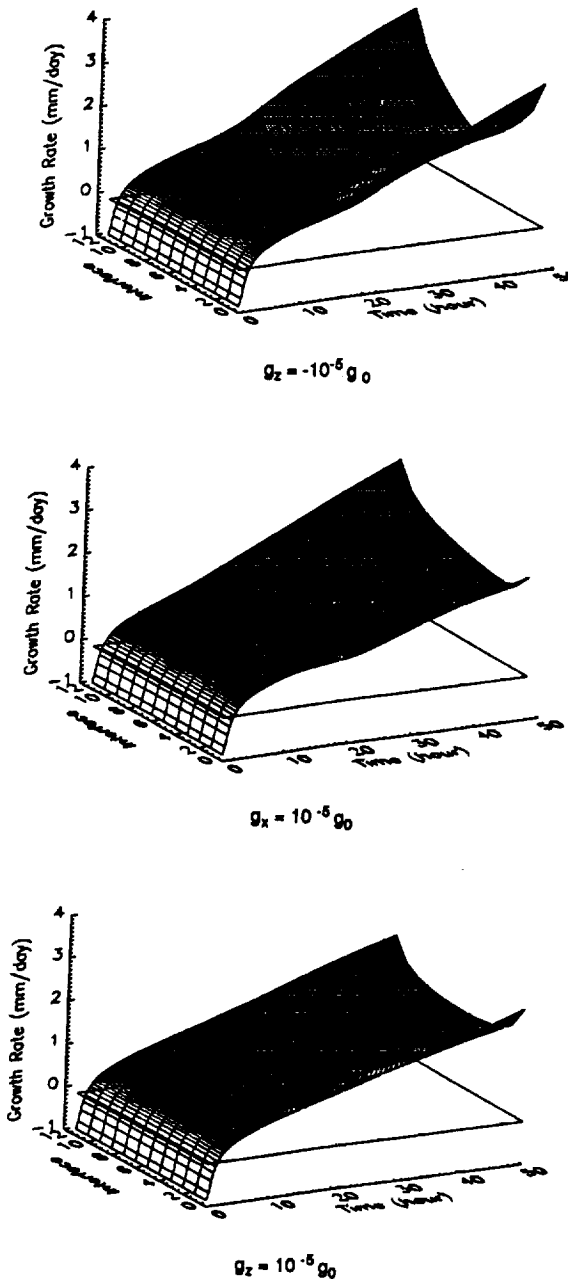

Fig. 5. Growth rate distribution of the (001) face with a *steady* background g in three orientations. The sting and the wall are cooled at a constant rate of 0.42°C/h for 50 h. The annotation "Interface" denotes the interface positions of the (001) face in x direction.

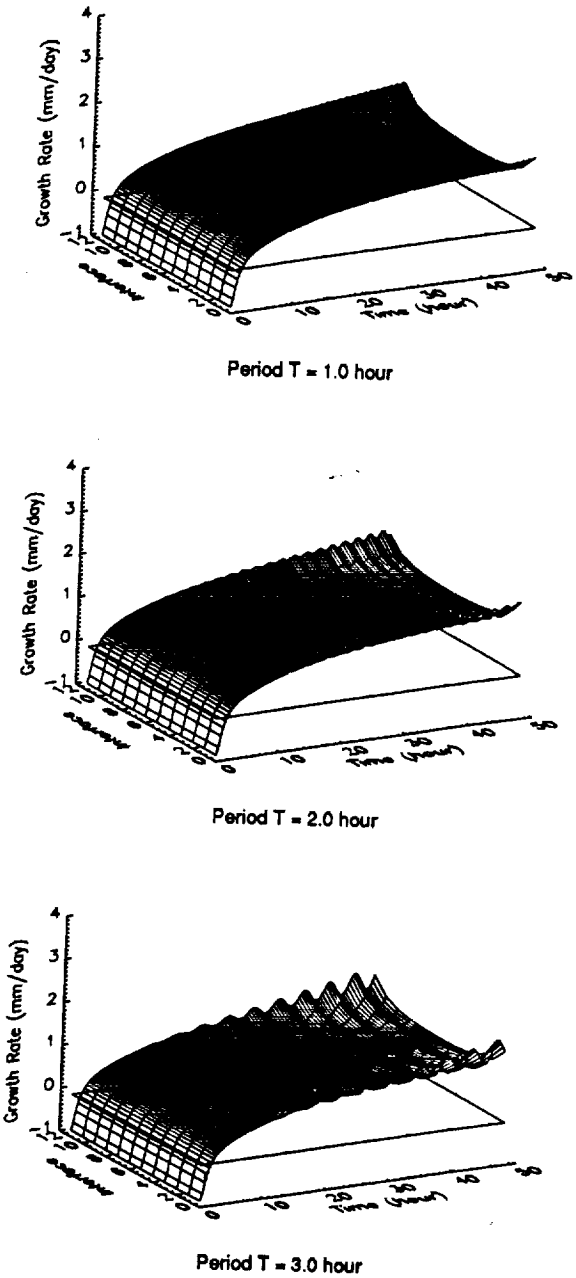

Fig. 6. Growth rate of the (001) face with a background g *rotating* at three different frequencies. The sting and the wall are cooled at a constant rate of 0.42°C/h for 50 h. The annotation "Interface" denotes the interface positions of the (001) face in x direction.

becomes symmetric and almost uniform. Although the nutrient solution becomes depleted as it approaches the corner, the concentration gradient increases. These two effects are so well balanced that the growth rate is nearly uniform along the face. Furthermore, since the depleted solution is driven to the lower part of the cell, the concentration of the approaching flow varies much less with space and time than the other two cases. For long experiments, the iso-concentration lines become flatter,

i.e. more parallel to the crystal face. If the cell has a large enough space in the lower region, it becomes a reservoir for depleted solution, allowing the experiment to be prolonged to obtain a large crystal. We believe this is the best orientation for crystal growth in space.

It should be noted that non-uniform growth is inevitable with pure diffusion (no convection), because the concentration field then becomes sphere-like. Additionally, in the absence of convection, a much larger supercooling is needed to maintain a reasonable growth rate if a long experiment is required to obtain a large crystal. In many cases such a large supercooling is not permitted. Thus in comparison to 0 g, a very small steady background g, if properly oriented, can offer a better environment for crystal growth in space.

4.2. Inertial mode

For a Space Shuttle in the inertial mode, where the background g slowly rotates, Fig. 6 displays growth rates for three different frequencies of rotation. Since the convection cannot fully develop in a certain direction, its average influence will be smaller than when g is in a fixed orientation. Therefore, the average growth rate will be smaller. A fluctuation in growth rate, however, is inevitable. The magnitude of the fluctuation increases with the time period of the rotating g vector (i.e. the time the shuttle takes to orbit one cycle). This also means that the growth rate could be influenced when the space shuttle changes orientation in orbit.

4.3. Other factors

The temperature applied to the sting plays a critical role in controlling the growth process. The dotted lines in Fig. 3 show that if the cooling of the sting is stopped too early, the growth rate drops greatly (as occurred in Cell 3 of the Spacelab-3 experiment). The temperature on the cell wall, on the other hand, does not affect the growth significantly. Figure 7 shows a comparison of the average growth rate for two cooling methods: one in which both the sting and the wall are cooled at the same rate of 0.42°C/h for 50 h (called here "isothermal cooling"); the other in which only the sting is cooled as above while the wall is kept at the original temperature (46°C). The difference is very small. Thus, the influence of these two boundary conditions can be separated, with the temperature at the sting used to control the growth rate. The temperature on the wall can then be held higher in order to control the supercooling in the bulk solution to avoid spurious nucleation.

The case with the fast growing face exposed was also simulated. Figure 8 compares the average growth rate of the (010) face to the (001) face. Although the kinetic constant of the (010) face is double that of the (001) face, the average growth rate is only 10 to 20% larger for the (001) face. Although it is not known if using the fast growing face would cause unstable growth, this comparison indicates that the growth process is mainly controlled by mass transport.

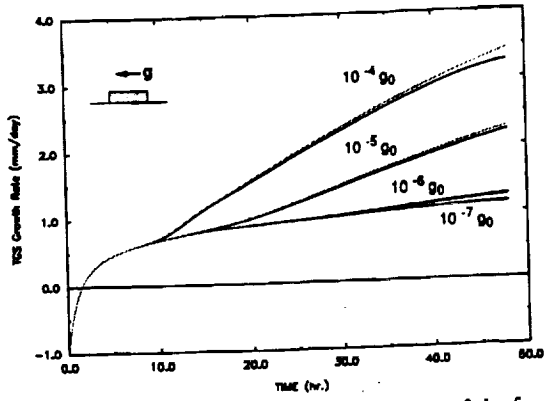

Fig. 7. Comparison of the average growth rate of the face (001) with two different cooling methods: (——) only the sting is cooled at a constant rate of 0.42°C/h while the wall is kept constant at the initial temperature (46°C); (-----) both the sting and the wall are cooled at a constant rate of 0.42°C/h for 50 h.

4.4. g-Jitter effect

g-Jitter was simulated by a sinusoidally varying body force superimposed on a steady background g of $10^{-6} g_0$. The magnitude used was $10^{-3} g_0$. The frequencies were 1, 0.1, 0.01 Hz, and the orientation was tangent to the interface. To reduce the computational cost, g-jitter was added 10 h after the crystal began to grow under the steady background g. The transient response of growth rate to frequencies higher than 0.1 Hz was hardly seen. Consequently only the case of 0.01 Hz is shown here, in Fig. 9. Note that the fluctuation of the growth rate at the corners is much larger than in the center. The magnitude of the fluctuating growth rate increases as time goes on. The concentration distribution does not change significantly for a long time when g-jitter is applied. Figure 9 also shows that when g-jitter is applied, the time average growth rate becomes larger than when

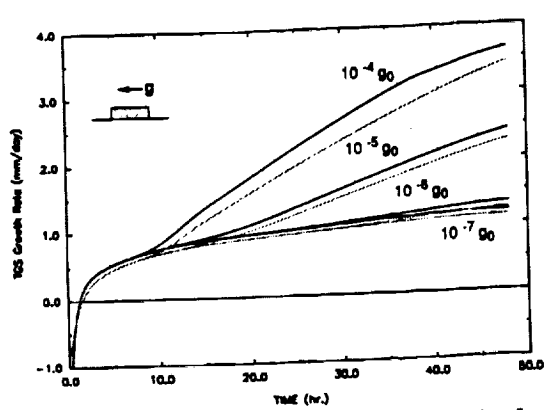

Fig. 8. Comparison of the average growth rate of a fast growing face (010) and a slow growing face (001). The sting is cooled at the rate of 0.42°C/h for 50 h while the wall is kept at 46°C. (——) The fast growing face (010). (-----) The slow growing face (001).

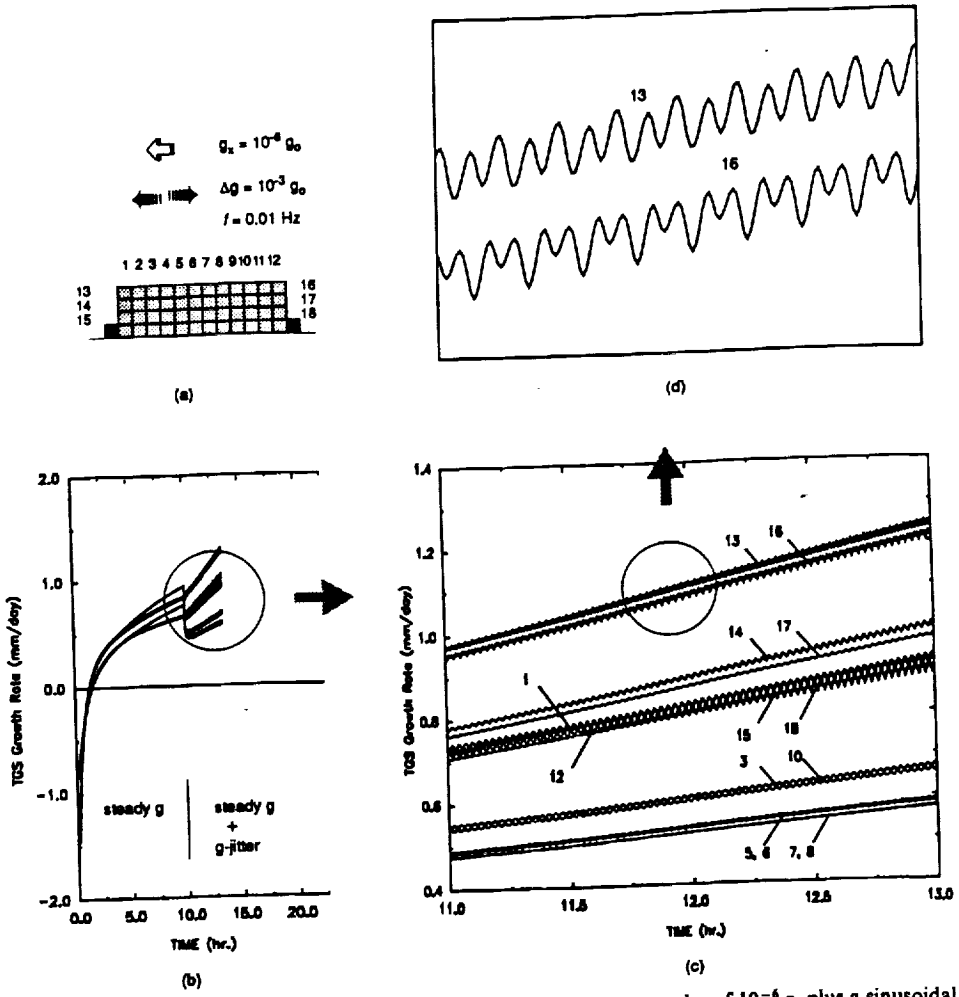

Fig. 9. Growth rate of the (001) face corresponding to a steady background g of $10^{-6} g_0$ plus a sinusoidal g-jitter of $10^{-3} g_0$ at 0.01 Hz. (a) The orientations of the steady g and g-jitter relative to the crystal surface and the index of the computation grid points at the interface. (b) To reduce the computational cost, g-jitter was superimposed on the steady background g 10 h after the crystal began to grow. (c) The numbers on the curves are the indices of computation grid points denoted in (a). The fluctuating magnitude of the growth rate at the corners (1, 12, 13, 16) are larger than in the center (5, 6, 7 and 8). (d) At the corners, the fluctuating growth rate had two peaks in each period.

only a steady background g is applied. Since the computational cost for small time steps was very high, limited simulations for g-jitter were carried out. Consequently the long term response to g-jitter is unclear. Nevertheless these results support the hypothesis that g-jitter caused the growth rate in the Spacelab 3 experiment to exceed that predicted for zero gravity.

Based on the above analysis, a temperature program for the sting was designed to control the average growth rate at 1.0 mm/day. The Shuttle was assumed to be in the gravity-gradient mode so that the orientation of the steady background g would be parallel to the exposed interface. Several likely cases were simulated. A sting/wall temperature ramp was chosen that gave good growth results over a broad range of steady g and g-jitter. Figure 10 shows that by using a proper temperature ramp, a steady growth rate near 1.0 mm/day can be maintained for a long time. Figure 11 shows the temperature ramp applied according to different situations. To quickly transit from dissolution to crystallization, a large cooling rate should be used for the initial several hours. When the growth rate reaches 1.0 mm/day, only a small temperature decline is needed to keep that constant growth rate. Instead of simulating the whole experiment with g-jitter signals, we also used a doubled diffusivity as in Ref. [10]. In these simulations, the maximum fluid velocity remains nearly constant after about 20 h of growth, but the concentration field never reaches a steady state.

5. CONCLUSIONS

In the bulk solution, weak thermal convection was established quickly. The convection converts to solutally dominated buoyancy-driven motion. The convection due to the steady background g is predicted

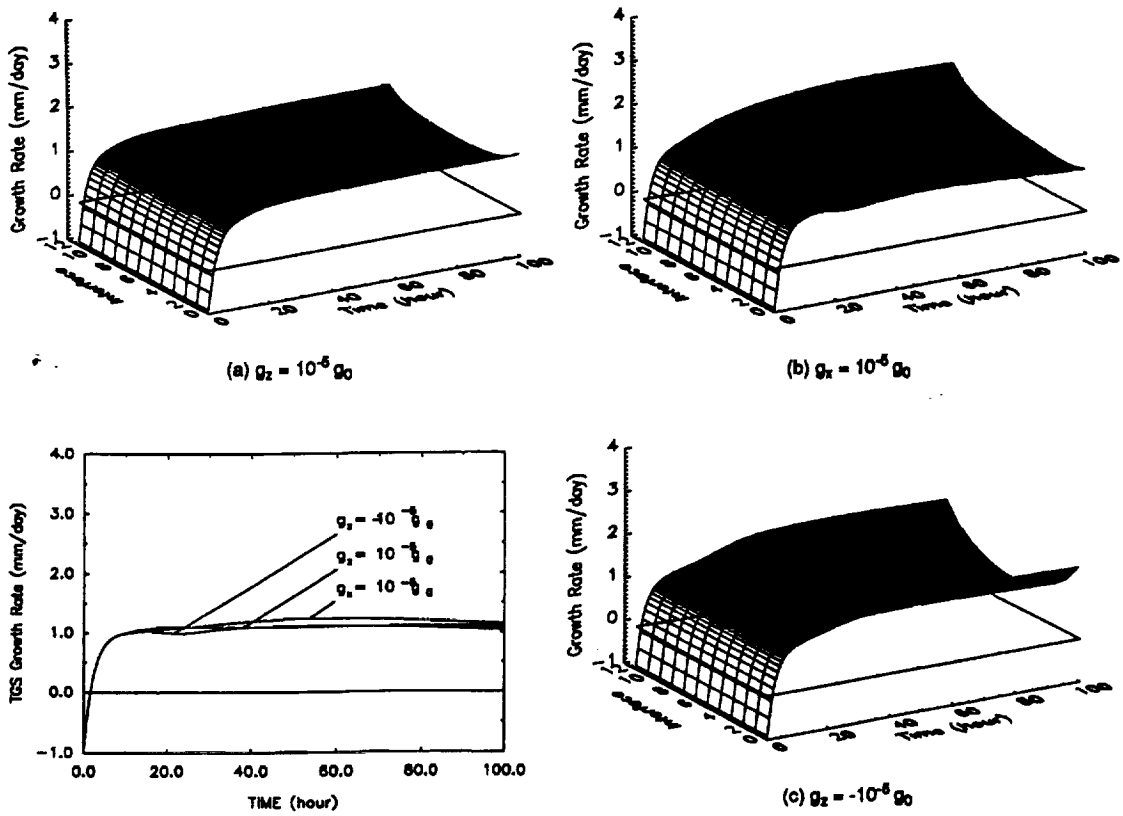

Fig. 10. Growth rate distribution along the (001) face (a–c) and the average growth rate with a steady g of $10^{-5} g_0$ in three different orientations. The temperature ramp at the sting was designed to control the average growth rate at about 1.0 mm/day.

to influence both the growth rate and the crystal morphology. The time required for buoyancy-driven convection to influence the growth rate depends on the magnitude of g, i.e. more time for smaller g. Under the same cooling condition, the average growth rate increases as the magnitude of g increases. A steady average growth rate of 1.0 mm/day can be reached when a properly designed temperature ramp

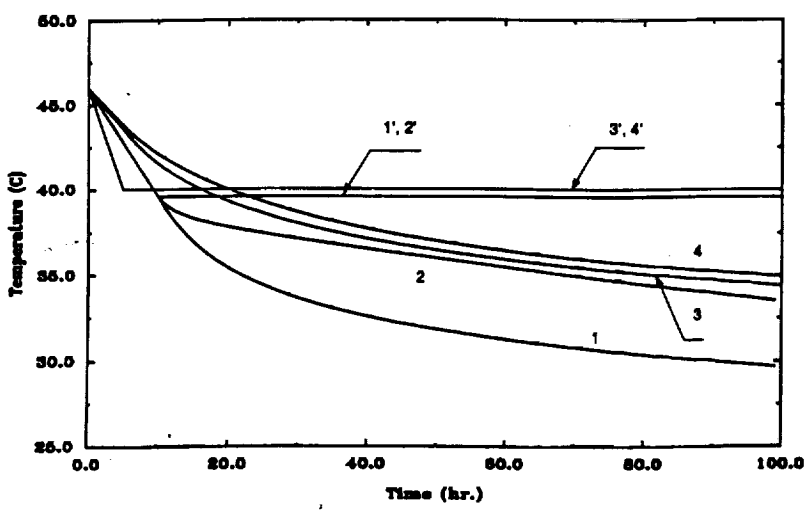

Fig. 11. Temperature applied to the sting and the wall to obtain an average growth rate of 1.0 mm/day. 1: $g = 1 \times 10^{-5} g_0$, (101) face, $D = 1.0$ (cm²/s); 2: $g = 510^{-5} g_0$, (101) face, $D = 1.0$ (cm²/s); 3: $g = 1 \times 10^{-5} g_0$, (101) face, $D = 2.0$ (cm²/s); 4: $g = 1 \times 10^{-5} g_0$, (110) face, $D = 2.0$ (cm²/s). Note: the diffusivity presented above are typical values. In simulation, D is the function of temperature and concentration. The curves 1′, 2′, 3′, 4′ above are the corresponding wall temperatures for cases 1, 2, 3, and 4.

is applied to the sting. The most uniform growth can be obtained when the g vector is aligned such that the solution flows normally toward the center of the crystal surface. The least uniform growth occurs for flow in the opposite direction. g-Jitter was found to have no transient effect when the frequency is higher than 0.01 Hz. g-Jitter at lower frequencies appeared to increase the growth rate, while the concentration distribution was little changed. The temperature at the sting determines the growth rate while the wall temperature has little effect. The growth process is mostly restrained by transport rather than by interface kinetics.

Acknowledgements—This work was supported by NASA through a sub-contract from Alabama A&M University. We are grateful to Professor Ravindra B. Lal of the Department of Physics at Alabama A&M University for his support and encouragement (he was the principal investigator on the IML experiment). We also appreciate helpful discussions with Professor Liya Regel here at Clarkson University and Dr J. Iwan D. Alexander at the Center for Microgravity and Materials Research of University of Alabama in Huntsville.

REFERENCES

1. R. B. Lal, A. Batra, W. R. Wilcox and J. D. Trolinger, A study of solution crystal growth in low-g (an experiment for IML-1 Mission). IML-1 Science Status Review, NASA Headquarters, Washington, D.C. (1990).
2. *First International Microgravity Laboratory*, The Payload Project Office of the NASA/Marshall Space Flight Center (MSFC), Huntsville, Alabama.
3. A. E. Roy, *Orbital Motion*. Adam Hilger, Bristol (1982).
4. L. Regel, Theoretical considerations on the characteristics of crystal growth under microgravity. *Materials Science in Space*. Halsted Press (1987).
5. H. Hamacher, B. Fitton and J. Kingdon, The environment of Earth-orbiting systems. In *Fluid Sciences and Materials Science in Space* (Edited by H. U. Walter). Springer, Berlin (1987).
6. H. D. Yoo, Computer simulation of triglycine sulphate crystal growth in space. Ph.D. dissertation, Clarkson Univ. (1986).
7. E. S. Nelson (Editor), An examination of anticipated g-jitters on space station and its effects on material processes. NASA Technical Memorandum, Lewis Research Center, Cleveland, Ohio (1991).
8. A. Authier, K. W. Benz, M. C. Robert and F. Wallrafen, Crystal growth from solutions. *Fluid Sciences and Materials Science in Space* (Edited by H. U. Walter). Springer, Berlin (1987).
9. L. C. Liu, W. R. Wilcox, R. Kroes and R. Lal, Modelling of TGS growth in space. *Material Processing in the Reduced Gravity Environment of Space* (Edited by G. E. Rindone). North-Holland, Amsterdam (1982).
10. H. D. Yoo, W. R. Wilcox, R. Lal and J. D. Trolinger, Modelling the growth of triglycine sulphate crystals in SpaceLab 3. *J. Cryst. Growth* **92**, 101–117 (1988).
11. A. Nadarajah, F. Rosenberger and J. I. D. Alexander, Modelling the solution growth of TGS crystals in low gravity. *J. Cryst. Growth* **104**, 218 (1990).
12. S. V. Patankar, *Numerical Heat Transfer and Fluid Flow*. Hemisphere, New York (1980).
13. *COMMIX-1B: A Three-Dimensional Transient Single-Phase Computer Program for Thermal Hydraulic Analysis of Single and MultiComponent Systems*, Vols 1 and 2. Argonne National Laboratory, Argonne, Illinois (1985).
14. W. R. Wilcox, Crystallization flow. *J. Cryst. Growth* **12**, 93–96 (1972).
15. W. R. Wilcox, A general treatment of mass transfer in crystal growth. In *Preparation and Properties of Solid State Materials* (Edited by W. R. Wilcox), Vol. 2. Marcel Dekker, New York, (1976).
16. R. L. Kroes and D. Reiss, Properties of TGS aqueous solution for crystal growth. *J. Cryst. Growth* **69**, 414–420 (1984).
17. R. L. Kroes, D. Reiss, E. Silberman and S. Morgan, Diffusion of triglycine sulfate in aqueous solution. *J. Phys. Chem.* **89**, 1657–1658 (1985).
18. Y. C. Chang and A. S. Myerson, Diffusivity of glycine in concentrated saturated and supersaturated aqueous solutions. *AICh.E. Jl* **32**, 1567–1569 (1986).

APPENDIX

Nomenclature

C = chemical species (mass %)
D = diffusion coefficient (m^2/s)
f = frequency (Hz)
g = acceleration (m/s^2)
g_0 = terrestrial gravitional acceleration, 9.80 (m/s^2)
h = enthalpy (J)
k = thermal conductivity (W/m · °C)
K_c = intervace kinetic coefficient (mm/day · °C)
n = unit length of the normal vector of the interface (m)
p = pressure (Pa)
t = time (s)
T = temperature (°C)
$\mathbf{u}$ = fluid velocity (m/s)
V = velocity at a boundary (m/s)
x = coordinates (m)
φ = phase angle
ρ = density (kg/m^3)
μ = viscosity (m^2/s)

Subscripts

c = crystal
eq = equilibrium or saturated state
f = fluid
i = interface
j = index of vector components
m = index of compontents of g-jitter
w = wall of the growth cell